

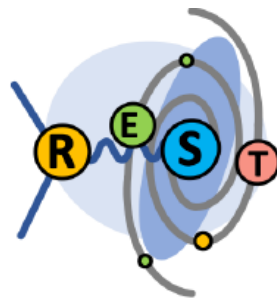
# Acceptance Study for BabyIAXO with REST

First edition

REST version v2.4.0

Johanna von Oy

23.08.2023



# Contents

<b>1</b>	<b>Introduction</b>	<b>1</b>
<b>2</b>	<b>Individual Component Acceptance</b>	<b>2</b>
2.1	Magnet . . . . .	3
2.2	XMM optics . . . . .	6
2.3	Detector . . . . .	8
2.4	Results internal rotation and movement . . . . .	11
<b>3</b>	<b>Gravitational Effects</b>	<b>12</b>
3.1	Magnet . . . . .	13
3.2	XMM optics . . . . .	14
3.3	Magnet and optics . . . . .	16
3.4	All (magnet, optics, detector) . . . . .	17
3.5	Results gravitational effects . . . . .	20
3.6	Overall rotation of the setup . . . . .	21

# 1 Introduction

One of the intended uses of the REST ray tracer, built by the IAXO collaboration, is to estimate the precision with which different components of the experiment have to be aligned. In this document, two different problems will be considered.

For one, the alignment acceptance of each component (magnet, optics, detector) will be derived as 99% efficiency of the total signal of a perfectly aligned system.

The other calculations are due to the deformation of the whole system, including the support structure, due to gravity. Both the detector and the magnet end are predicted to bend down depending on the angle BabyIAXO is rotated by.

In the following document, the results of the acceptance study are displayed in graphs and tables. Each data point in the graphs is the average of 9 simulations with 10000 events each, and the errors are derived from their standard deviation. Error bars have been limited to not reach above 100% because it is physically impossible for the rotated systems to have a relative efficiency of more than 1 as we define the optimal position to have an efficiency of 100%.

The fit function for each graph is done according to a s-function:

$$y = 0.5A \cdot \operatorname{erf} \left( \frac{x - \mu}{\sqrt{2}\sigma} \right) + 0.5A + B \quad (1)$$

## 2 Individual Component Acceptance

Each of the following components is turned individually around its own center downwards on the side facing away from the sun, as shown in Figure 2.

They are also moved downwards and, in the case of the magnet, sideways due to the inhomogeneity of the magnetic field.

At each of the positions the component is moved to, the flux arriving at the detector is calculated as the multiplication of the axion coupling to a photon in the magnetic field, the probability of the photon transmitting through the medium in the magnet bore (here vacuum), the transmission through the flange between the magnet bore and the optics, the probability of the photon being reflected on the mirrors of the optics and the probability of it transmitting through the vacuum-tight window in front of the detector.

For the individual components, the efficiency of interest that is mentioned is always at 99% of the efficiency of the optimal position because if all component efficiencies are then multiplied by each other (magnet rotation and displacement, optics rotation and displacement and detector displacement) the total efficiency would be 95%.

The coordinate system is shown in Figure 1, with its origin at the downstream (facing away from the sun) flange of the magnet and the X-ray optics center at  $z=1200$  mm.

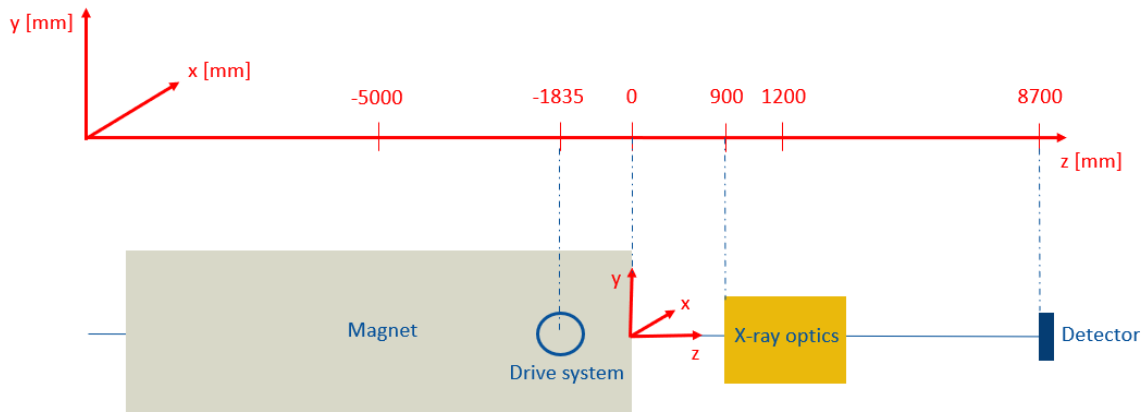


Figure 1: Coordinate system with its origin at the downstream flange of the magnet

The setup simulated here is the magnetic field design shown in Figure 3. The XMM optics center is positioned to the downstream flange of the magnet at a distance of 900 mm, and the detector window is in its focal plane. In this case, a detector window made of 300 nm Si<sub>3</sub>N<sub>4</sub> with a radius of 7 mm has been used with a striped Si strong back.

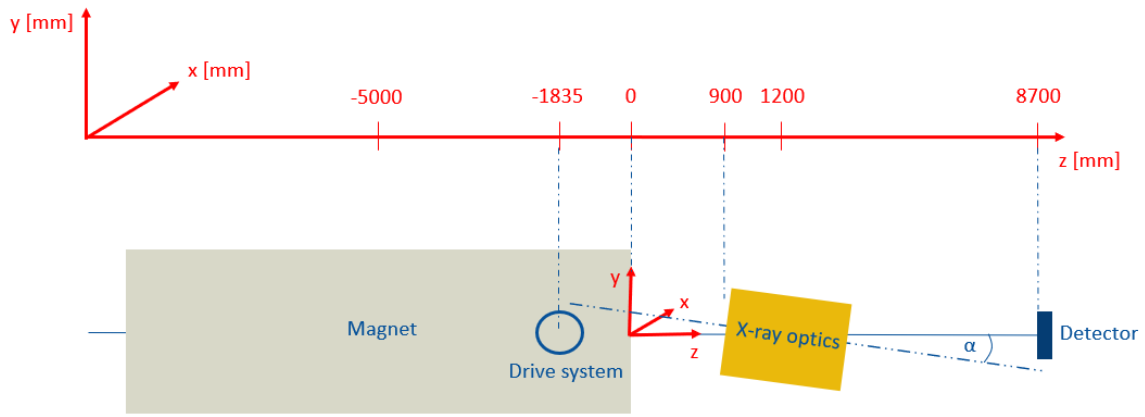


Figure 2: Coordinate system with the optics turned around its center

## 2.1 Magnet

In the following, only the magnet will be moved while the other components stay in place. The loss of efficiency due to the magnet's rotation around its own center downwards and to the side is shown in Figure 4 and 5. Figure 6 depicts the effects of the magnet moving in negative y-direction, i.e. downwards, while Figure 7 shows the same for the magnet moving in negative x-direction.

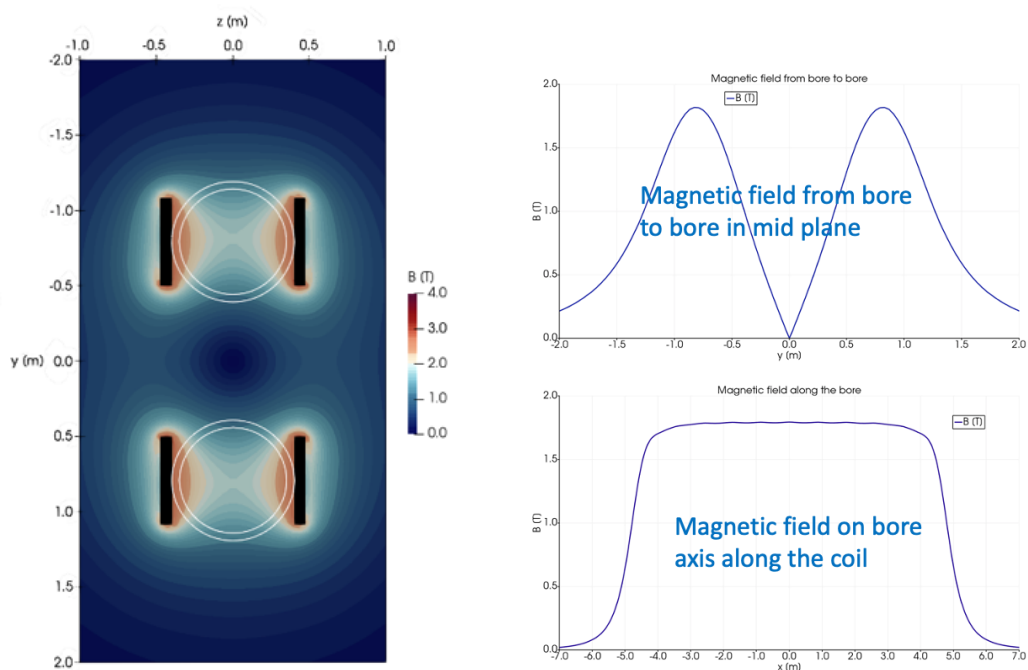


Figure 3: Magnetic field as of the current planning status. In the cross section (upper left) of the bore it is visible, that it is not radial symmetric

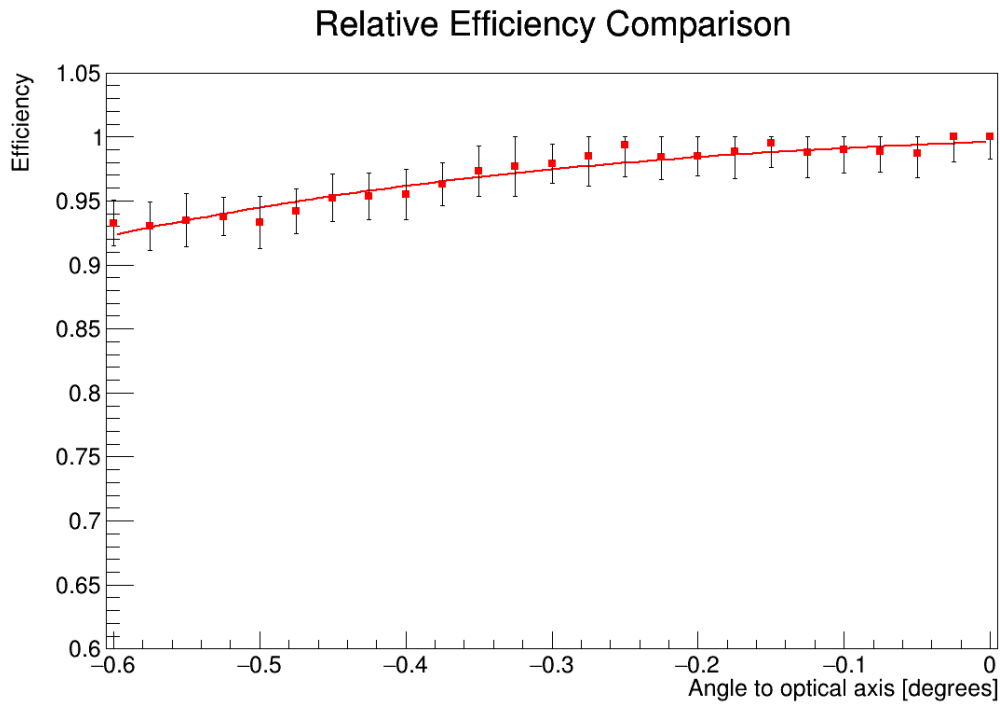


Figure 4: Efficiency of the magnet depending on the angle it is turned around its own center downwards (pitch). 99% efficiency reached at  $\alpha_{\text{pitch}} = -0.12^\circ$  (which coincides with  $\Delta y = -10.1$  mm at the center of the magnet's entrance)

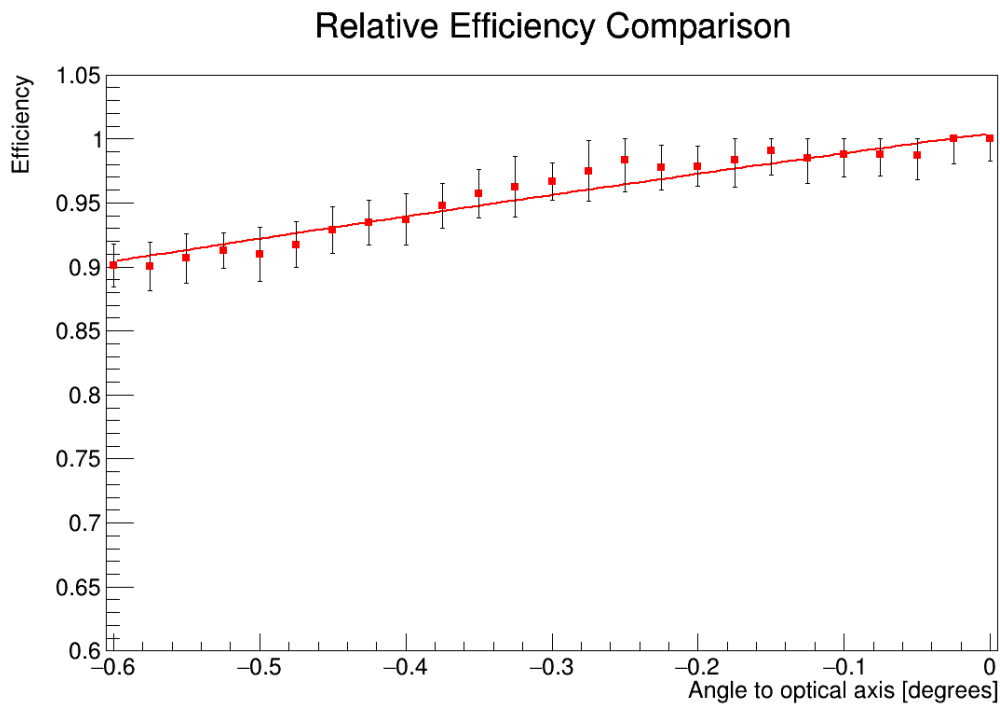


Figure 5: Efficiency of the magnet depending on the angle it is turned around its own center to the side (yaw). 99% efficiency reached at  $\alpha_{\text{yaw}} = -0.09^\circ$  (which coincides with  $\Delta x = -7.8$  mm at the center of the magnet's entrance)

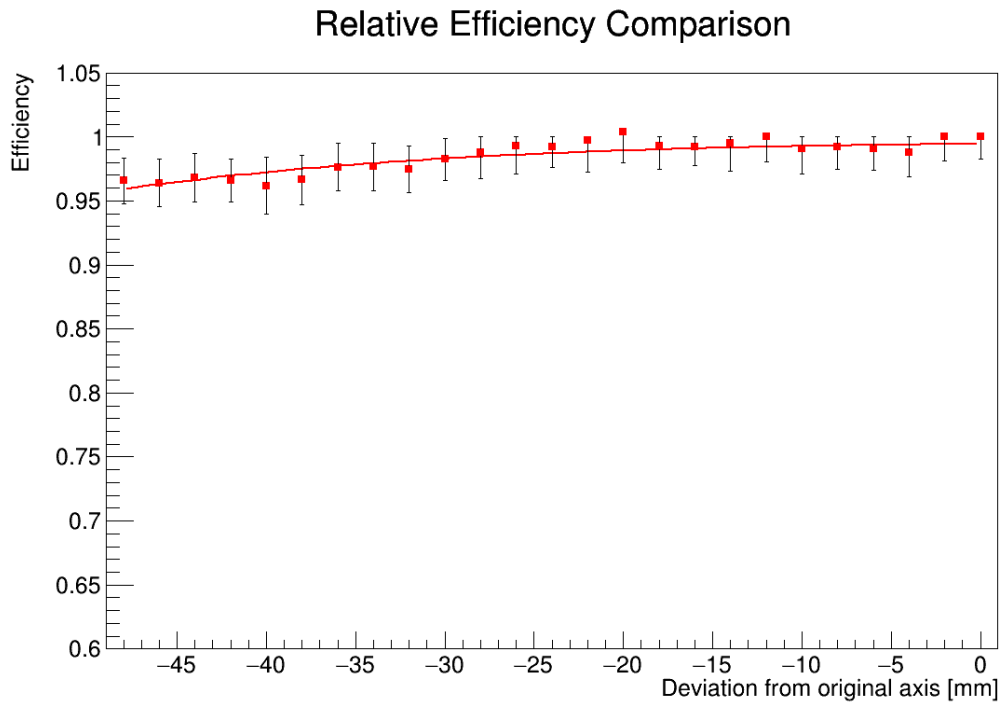


Figure 6: Efficiency of the magnet depending on its deviation from the optimal position downwards. 99% efficiency reached at  $y = -24.76$  mm

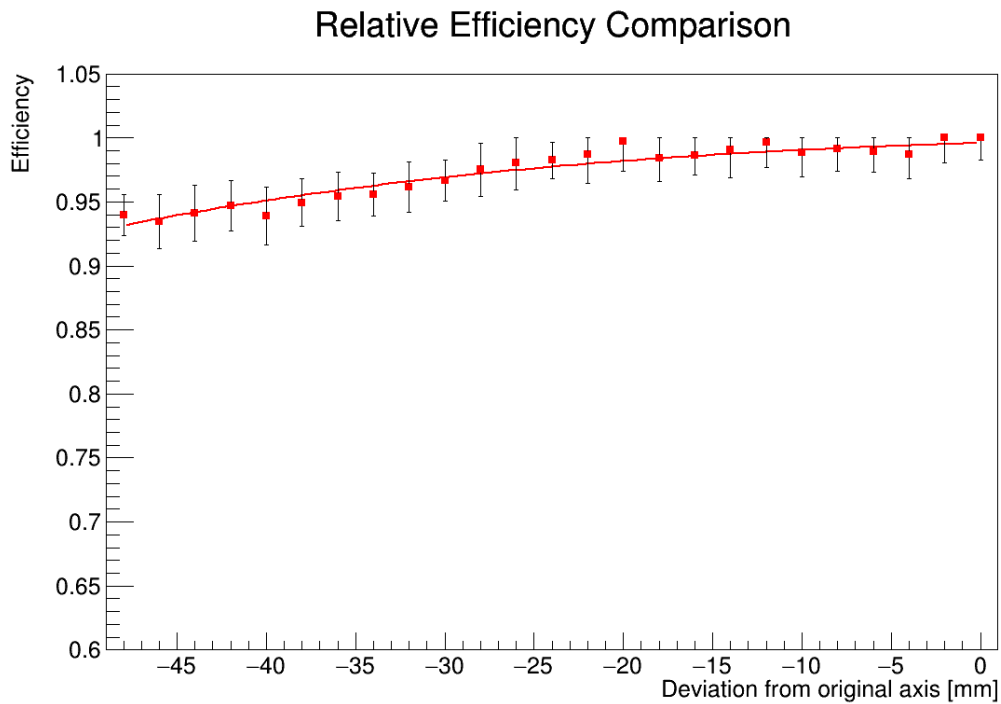


Figure 7: Efficiency of the magnet depending on its deviation from the optimal position to the side. 99% efficiency reached at  $x = -10.5$  mm

## 2.2 XMM optics

In this part, only the X-ray optics is moved while all other components stay in optimal position. In Figure 8 the XMM optics is rotated around its own center at  $z = 1200$  mm downwards, and in Figure 10 it is rotated to the side. In Figure 11 it is moved in negative y-direction and in Figure 12 in negative x-direction.

Figure 9 shows the distribution of X-rays at the focal plane at a rotation of the optics of  $\alpha = -0.12^\circ$ . Here it is recognizable that if only the optic is rotated around its center and the other components stay in optimal position, the focal point doesn't move out of the detector window.

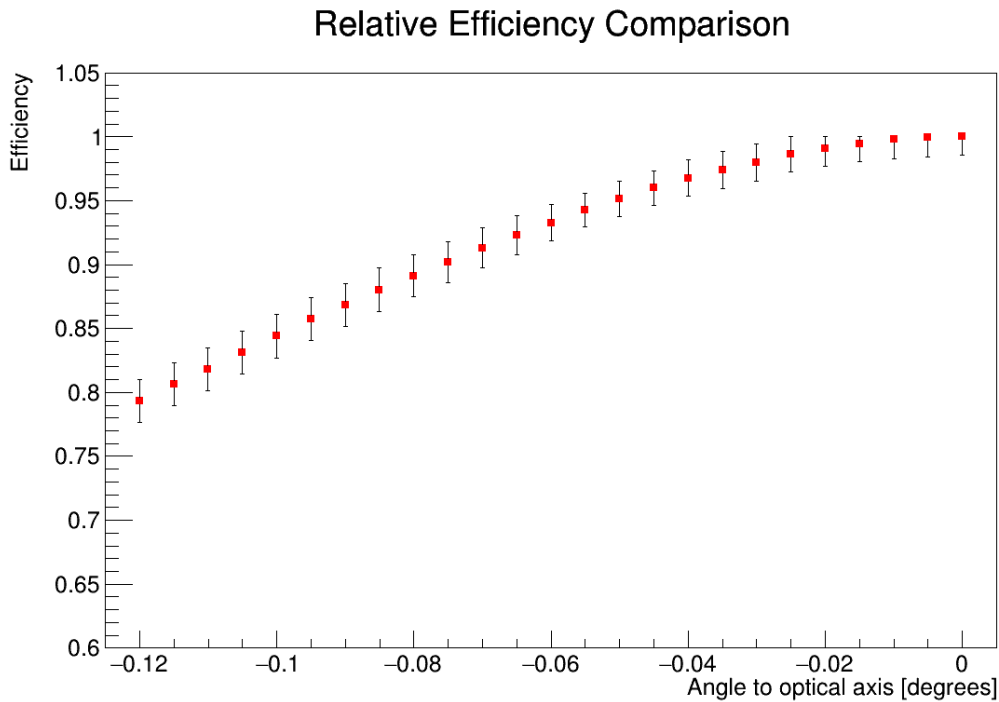


Figure 8: Efficiency of the XMM optics depending on the angle it is turned around its own center downwards. 99% efficiency reached at  $\alpha_{\text{pitch}} = -0.021^\circ$  (which coincides with  $\Delta y = -0.11$  mm at the center of the optics' entrance)

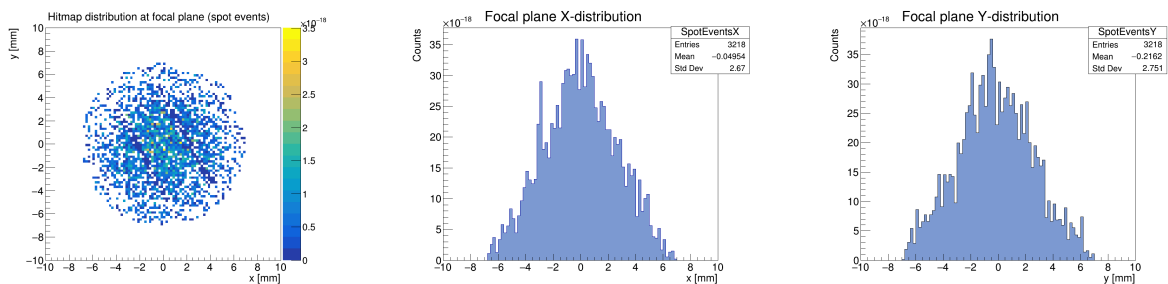


Figure 9: Distribution at the focal plane at a rotation of the XMM optics of  $\alpha = -0.12^\circ$  around its center

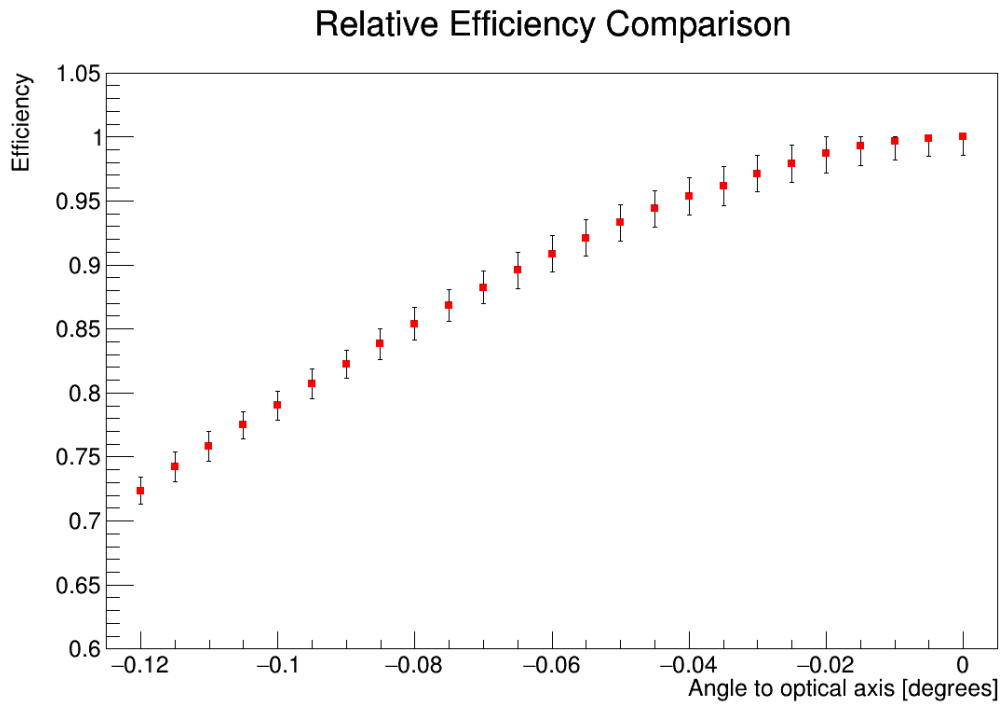


Figure 10: Efficiency of the XMM optics depending on the angle it is turned around its own center sideways. 99% efficiency reached at  $\alpha_{\text{yaw}} = -0.017^\circ$  (which coincides with  $\Delta y = -0.09$  mm at the center of the optics' entrance)

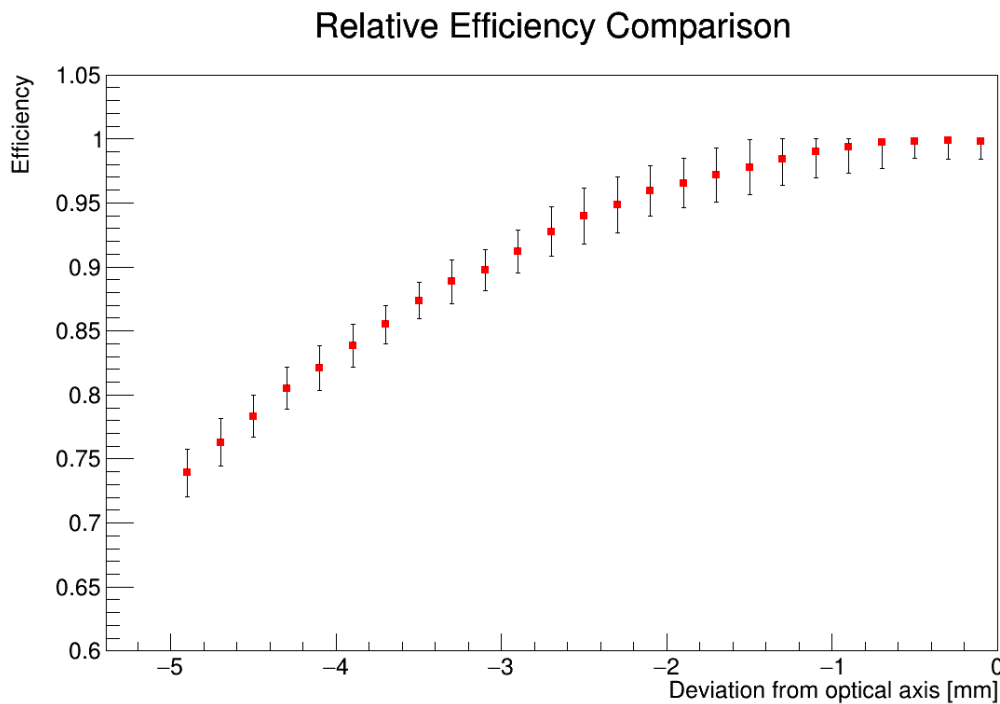


Figure 11: Efficiency of the XMM optics depending on its deviation from the optimal position downwards. 99% efficiency reached at  $y = -1.09$  mm

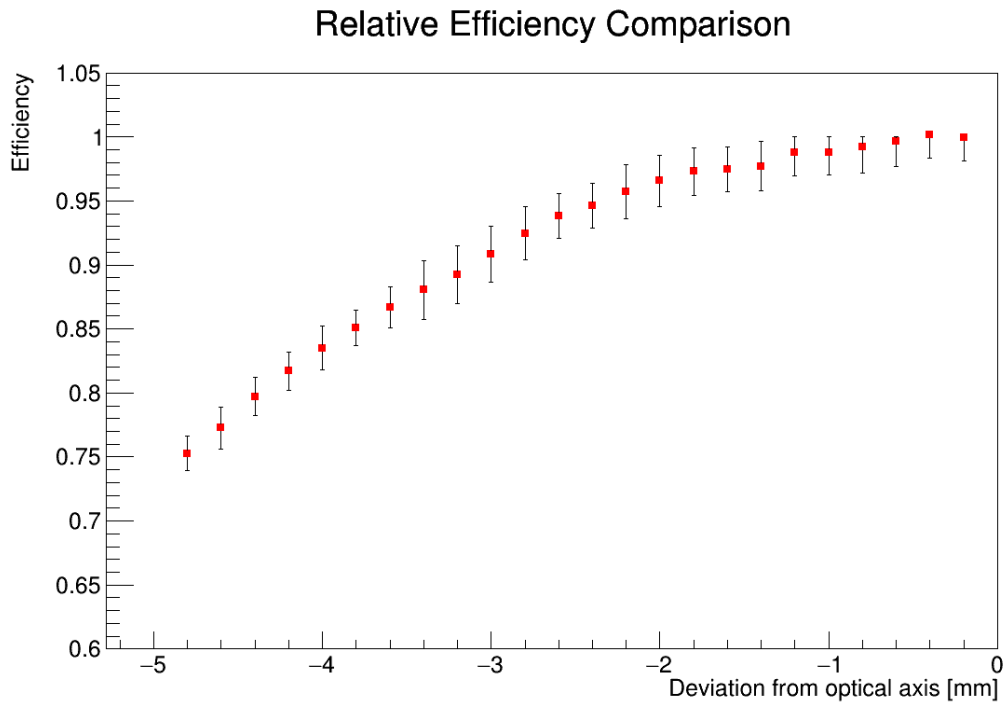


Figure 12: Efficiency of the XMM optics depending on its deviation from the optimal position sideways. 99% efficiency reached at  $y = -1.02$  mm

### 2.3 Detector

In the following, the detector, which is so far simulated as the vacuum-tight window, is moved in negative y-direction (Figure 13) and negative x-direction (Figure 14) while the other components stay in the optimal position. In addition to this, the same movements have been done with a 3.5  $\mu\text{m}$  thick mylar ( $\text{C}_{10}\text{H}_8\text{O}_4$ ) window with a radius of 8.5 mm and a strongback made out of copper. The efficiency loss of this is shown in Figure 15 and Figure 16.

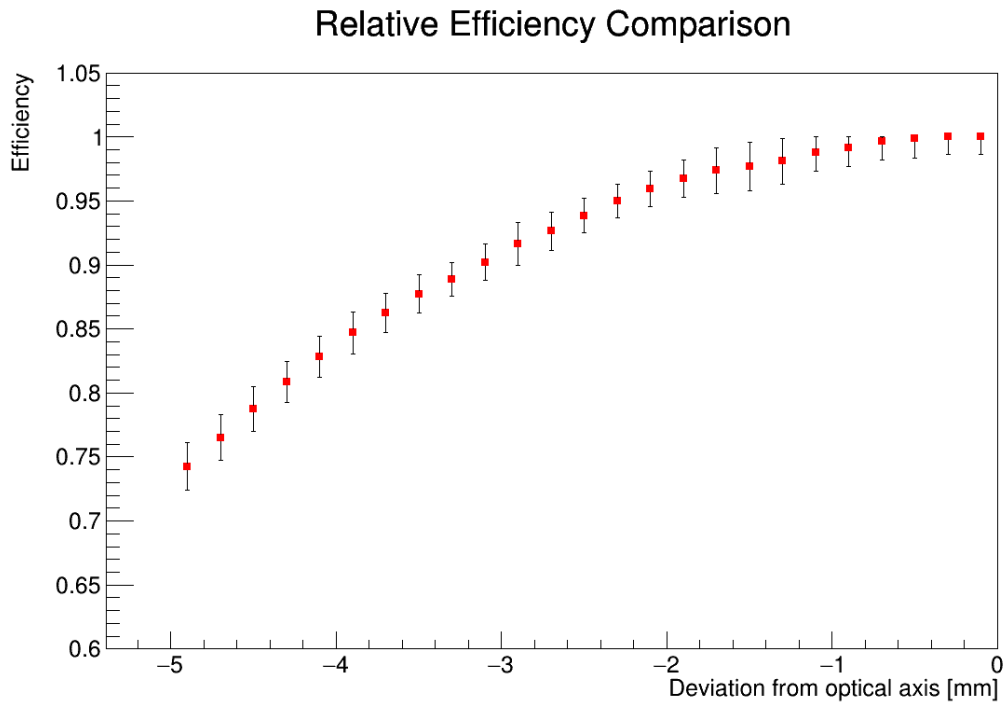


Figure 13: Efficiency of the GridPix detector window depending on its deviation from the optimal position downwards. 99% efficiency reached at  $y = -1.04$  mm

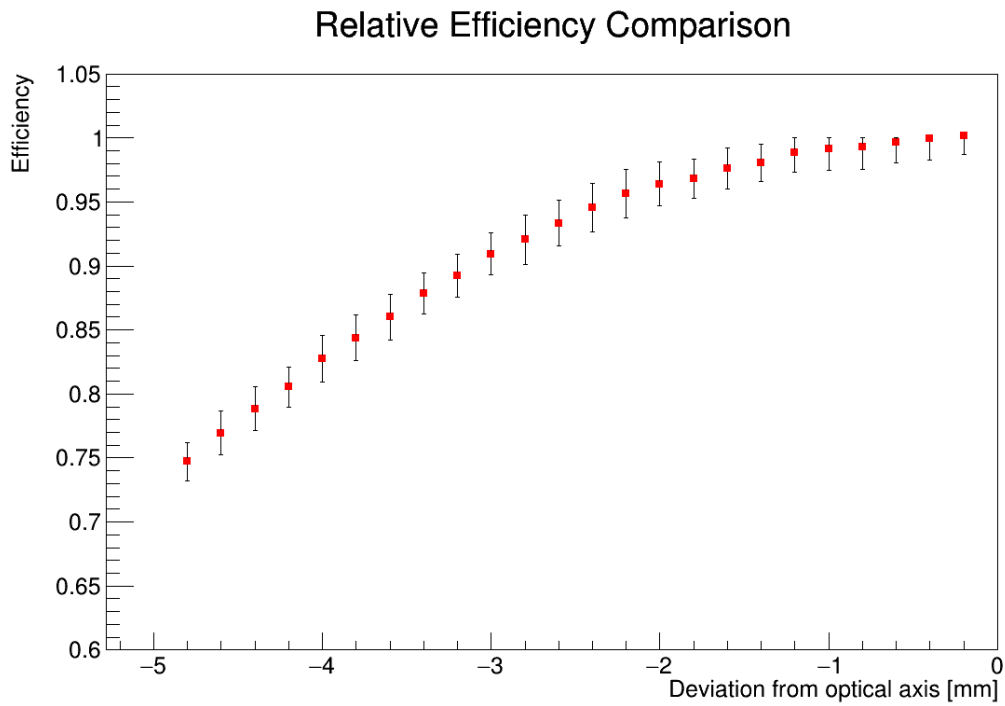


Figure 14: Efficiency of the GridPix detector window depending on its deviation from the optimal position sideways. 99% efficiency reached at  $y = -1.06$  mm

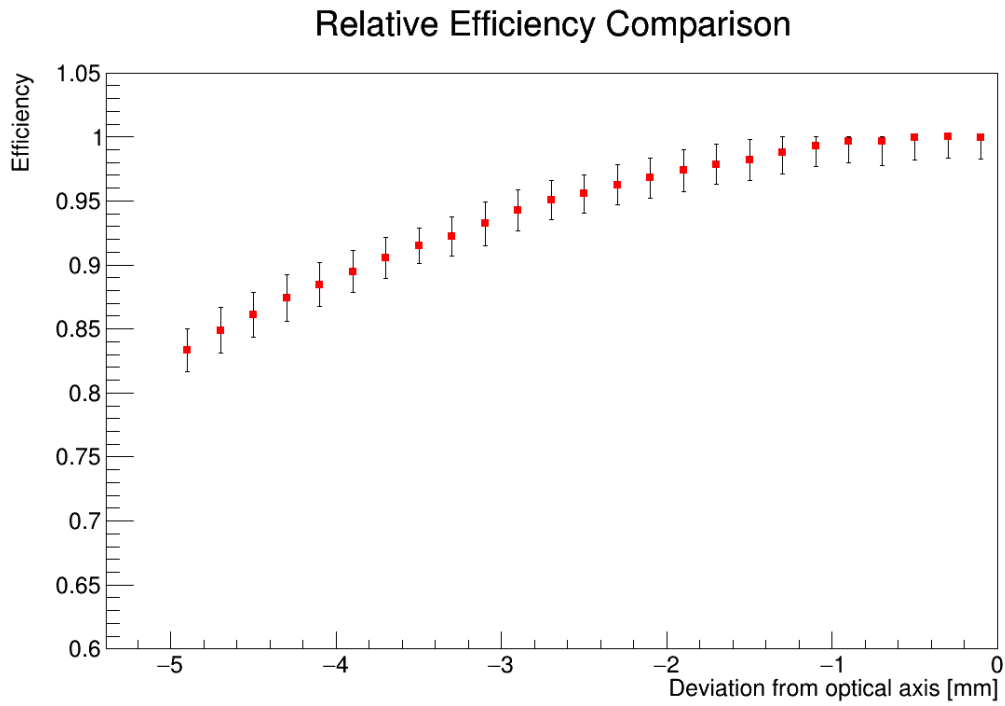


Figure 15: Efficiency of the Micromegas detector window depending on its deviation from the optimal position downwards. 99% efficiency reached at  $y = -1.22$  mm

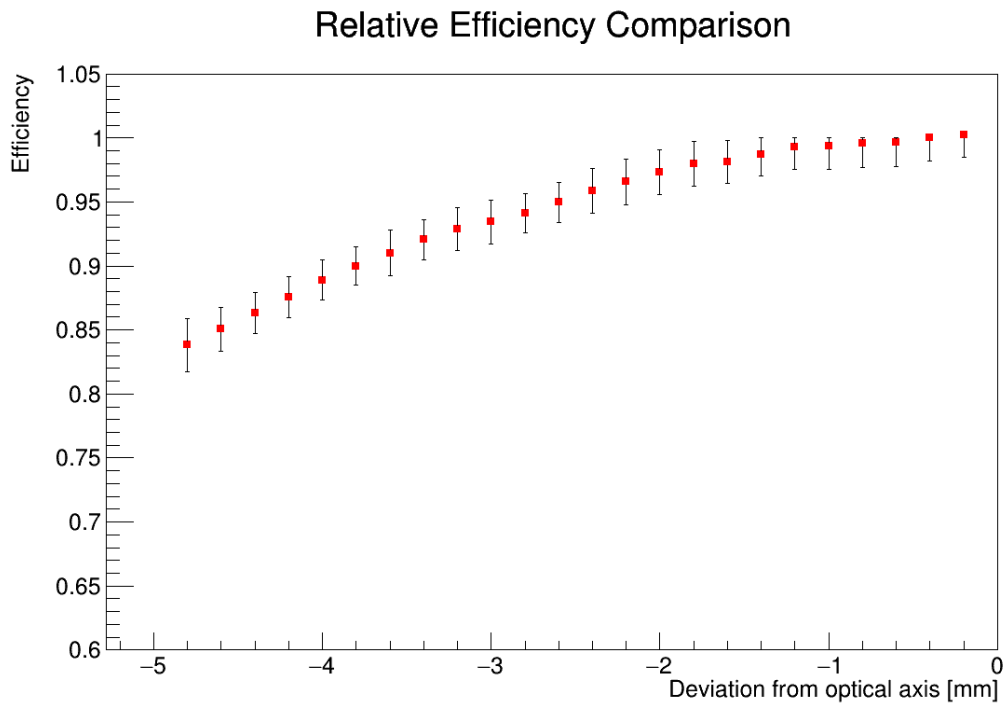


Figure 16: Efficiency of the Micromegas detector window depending on its deviation from the optimal position sideways. 99% efficiency reached at  $y = -1.25$  mm

## 2.4 Results internal rotation and movement

In the following Table 1, the individual acceptances of the components are shown due to their loss of 1% efficiency after rotation around their center or movement. Here it is crucial to understand that this doesn't reflect a performance loss due to combinations of rotation and movement because that could have other effects.

It is also important to note that the described detector window (see beginning of 2) that has been used makes the simulation not energy independent, as its transmission depends on the X-ray's energy. This could have an effect when the rotation of the optics changes the reflected X-rays' energy distribution.

Individual acceptance magnet	
Rotation $\alpha_{\text{pitch}}(99\%)$ [ $^\circ$ ]	Rotation $\alpha_{\text{yaw}}(99\%)$ [ $^\circ$ ]
-0.19	-0.13
Deviation $y(99\%)$ [mm]	Deviation $x(99\%)$ [mm]
-24.76	-17.77

Individual acceptance XMM optics	
Rotation $\alpha_{\text{pitch}}(99\%)$ [ $^\circ$ ]	Rotation $\alpha_{\text{yaw}}(99\%)$ [ $^\circ$ ]
-0.021	-0.017
Deviation $y(99\%)$ [mm]	Deviation $x(99\%)$ [mm]
-1.09	-1.02

Individual acceptance detector	
$y(99\%)$ GridPix window [mm]	$x(99\%)$ GridPix window [mm]
-1.04	-1.06
$y(99\%)$ Micromegas window [mm]	$x(99\%)$ Micromegas window [mm]
-1.22	-1.25

Table 1: The values of  $\alpha$  and  $y$  for the individual rotations and movements of the different BabyIAXO components where the flux arriving at the detector is 99% from the flux at the optimal position

### 3 Gravitational Effects

For the simulation of the gravitational effects, the components are turned around the point where the support structure is mounted to the drive system, which is going to be assumed to be at  $z = -1835$  mm. The deviation plots are unnecessary for the individual components here because they are the same as in the last section.

In Figure 17, a preliminary simulation from early 2022 of the effects of the deformation of the setup due to gravity are shown for the position where it is parallel to the ground. Those in itself can be compensated for easily, but there are different deformations for the maximal positions of  $-25^\circ$  and  $25^\circ$  to the ground. The difference between these deformations at the outermost points of the setup are displayed in Figure 18 and are less easily compensable.

For the magnet side, the difference is, on average, over different simulation methods 0.7 mm and for the detector side 1.6 mm.

Since the study has been conducted by turning the objects around the point where the support structure is mounted to the drive system, the difference to the optimal position at the far ends of the setup can be calculated with  $\Delta y = \tan(\alpha) \cdot \Delta z_i$ . For the magnet side, the distance to the point where the drive system is mounted to the outermost point is  $\Delta z_M = 8165$  mm, and for the detector side, it is  $\Delta z_D = 10\,535$  mm.

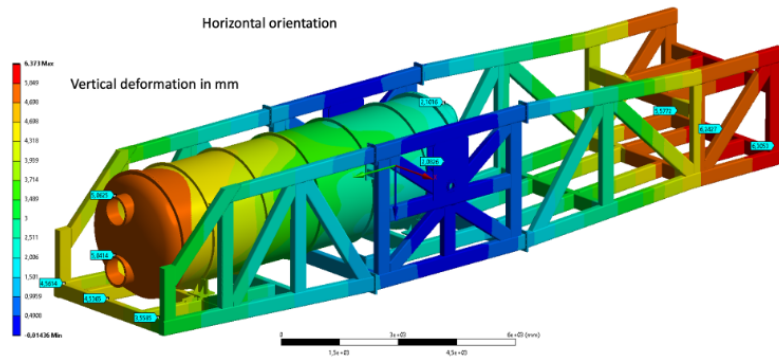


Figure 17: The simulated deformation of the BabyIAXO setup due to gravity at a rotation angle of  $0^\circ$

Support Frame Deformations (mm)						
Magnet side						
Tilt	Ansys <sup>a)</sup>	Ansys <sup>b)</sup>	Comsol	RStab	Average	Std Dev
0°	4.5	4.1	3.9	4.9	4.4	0.4
25°	4.6	3.9	3.8	4.9	4.3	0.5
-25°	3.5	3.6	3.3	3.8	3.5	0.2
$\Delta(25 - 0)$	0.1	-0.2	-0.1	0.0	-0.1	0.1
$\Delta(-25 - 0)$	-1.0	-0.5	-0.6	-1.1	-0.8	0.3
Detector side						
Tilt	Ansys <sup>a)</sup>	Ansys <sup>b)</sup>	Comsol	RStab	Average	Std Dev
0°	6.2	6.0	5.9	4.8	5.8	0.1
25°	4.4	5.3	4.3	3.0	4.3	0.4
-25°	6.4	5.6	6.1	5.3	5.9	0.4
$\Delta(25 - 0)$	-1.8	-0.7	-1.6	-1.8	-1.5	0.5
$\Delta(-25 - 0)$	0.2	-0.4	0.2	0.5	0.1	0.3

Figure 18: The simulated deformation of the BabyIAXO setup due to gravity at different rotation angles

### 3.1 Magnet

In the following Figure 19 the effects of the magnet's rotation around the point where the drive system is mounted to the support structure is shown. All other components stay in optimal position.

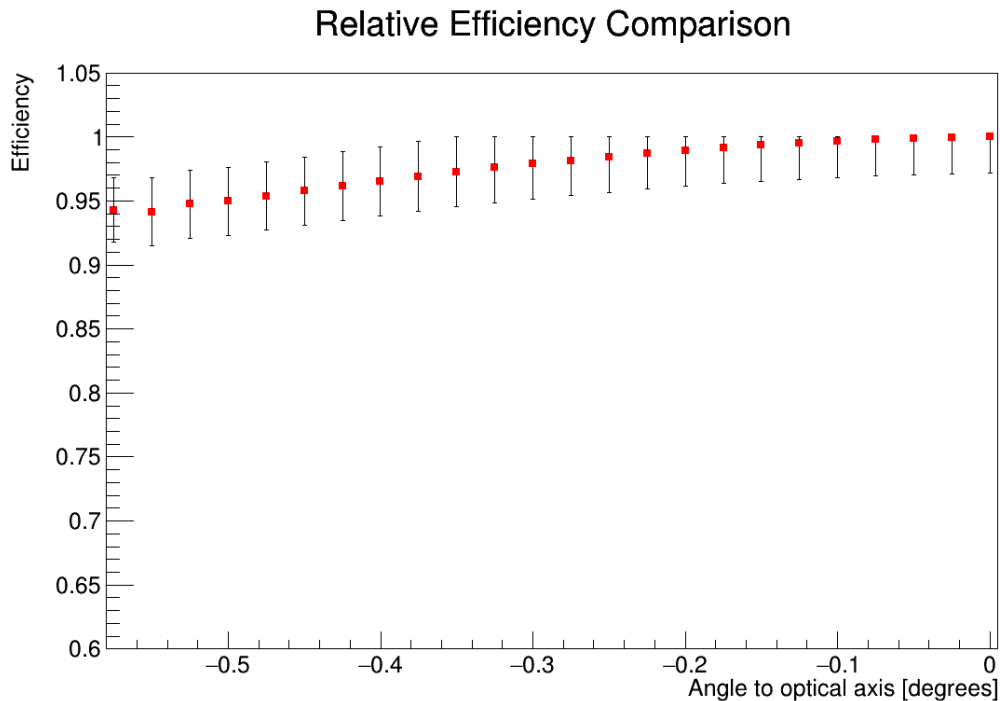


Figure 19: Efficiency of the magnet depending on the angle it is turned around the systems center downwards. 99% efficiency reached at  $\alpha = -0.19^\circ$  ( $\Delta y = -27.25$  mm at  $z = -10$  m)

### 3.2 XMM optics

In this part, the XMM optics is turned around the point where the drive system is mounted to the support structure while all other components stay in optimal position, a schematic view of which can be seen in Figure 20. The loss of efficiency due to that is shown in Figure 21.

The focal plane distribution is depicted in Figure 22 at the same angle of  $\alpha = -0.12^\circ$  as Figure 9. As a difference, it is clearly visible that a rotation of the optics around a point different than its center moves the focal spot from the detector that stayed in its original position. This is due to the fact that the focal spot moves in x- and y-direction the same way the center of the optics moves. To correct this, the detector would have to be moved downwards.

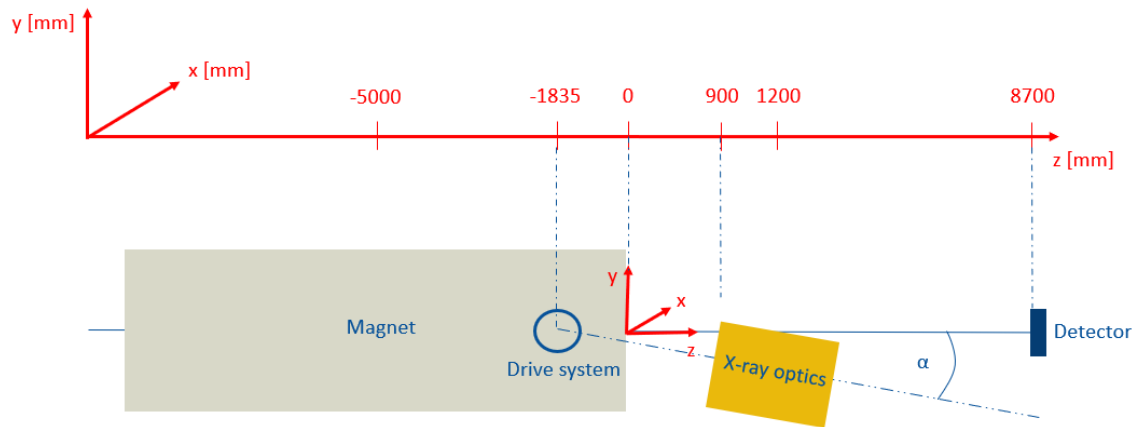


Figure 20: Coordinate system with the optics turned around the systems center

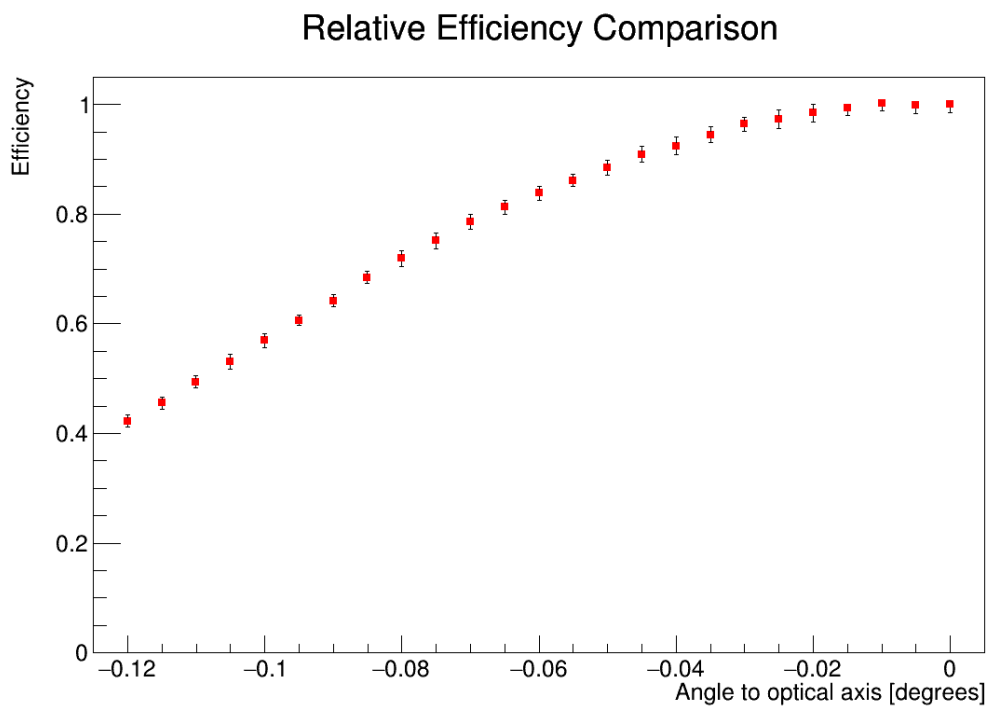


Figure 21: Efficiency of the XMM optics depending on the angle it is turned around the systems center downwards. 99% efficiency reached at  $\alpha = -0.0175^\circ$  ( $\Delta y = -3.22$  mm at  $z = 8.7$  m)

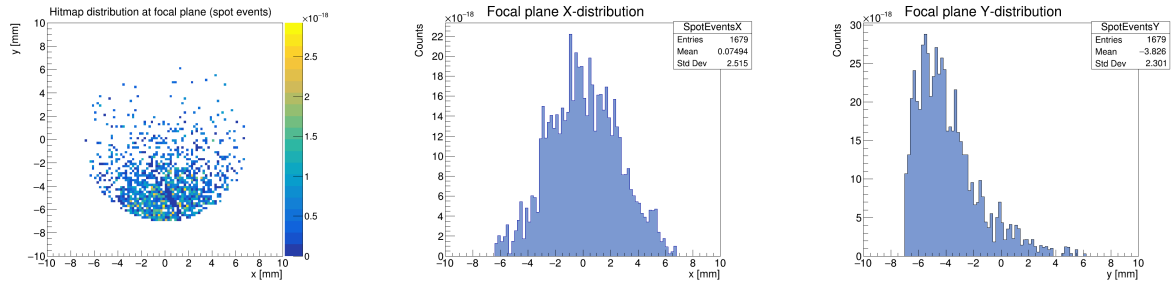


Figure 22: Distribution at the focal plane at a rotation of the XMM optics of  $\alpha = -0.12^\circ$  around the systems center

### 3.3 Magnet and optics

As can be seen in Figure 23, in the following, the magnet and the XMM optics are turned around the point where the drive system is mounted to the support structure while the detector stays in optimal position. The effects of those two components turned in different directions around the same angle  $\alpha$  can be seen in Figure 24.

Figure 25 shows the distribution of X-rays at the focal plane at a rotation angle of  $\alpha = -0.06^\circ$  around the system's center. The angle is only half as big as in Figure 22, but a similar effect can be seen.

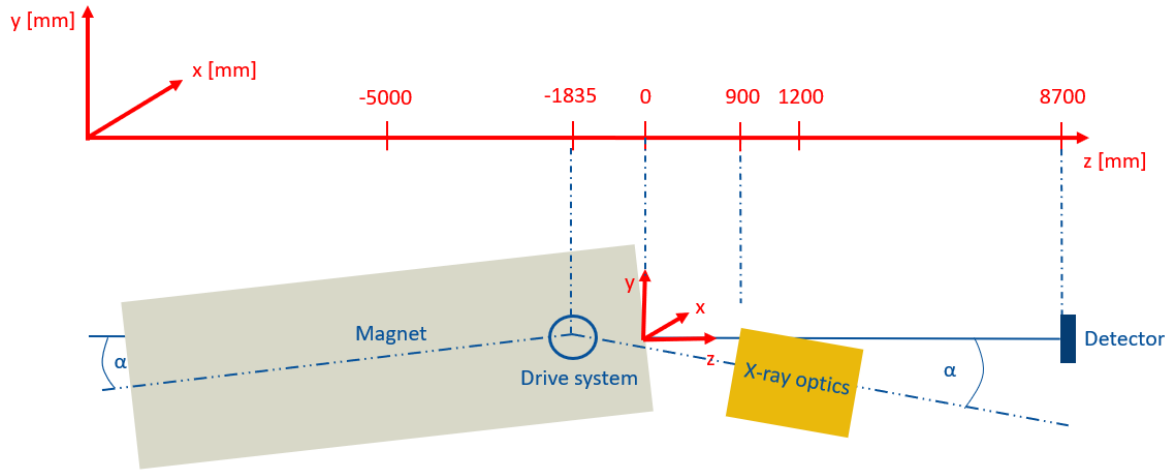


Figure 23: Coordinate system with the deformation effects due to gravity but correction of the detector upwards

## Relative Efficiency Comparison

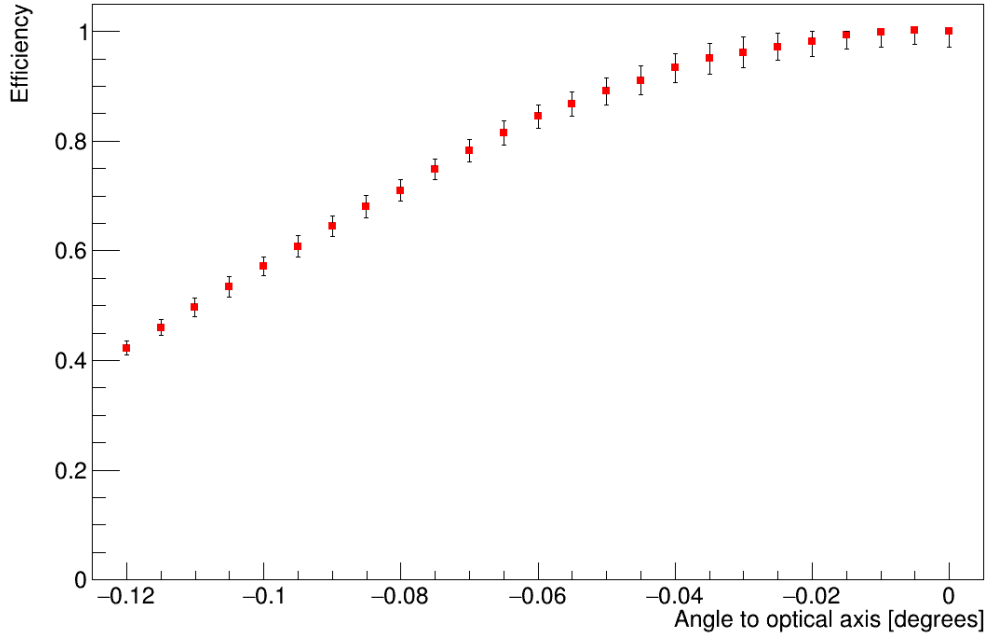


Figure 24: Efficiency of the XMM optics and the magnet depending on the angle they are both turned around the systems center like a banana but the detector stays in optimal position. 99% efficiency reached at  $\alpha = -0.016^\circ$  and 95% efficiency reached at  $\alpha = -0.035^\circ$  ( $\Delta y = -6.38$  mm at  $z = 8.7$  m and  $\Delta y = -4.94$  mm at  $z = -10$  m)

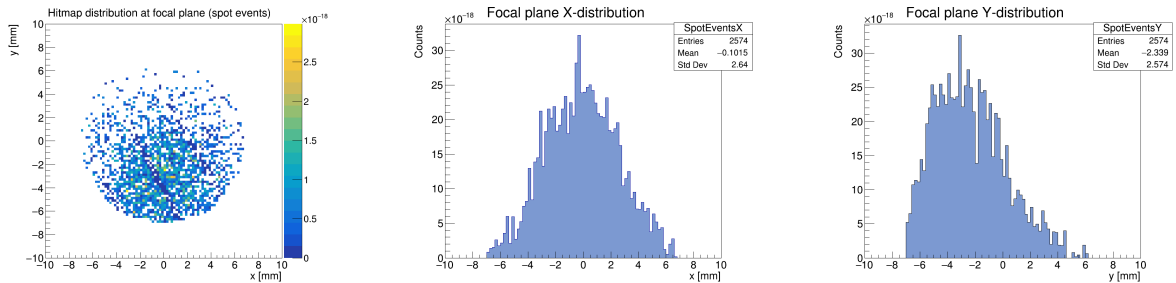


Figure 25: Distribution at the focal plane at a rotation of magnet and optics of  $\alpha = -0.06^\circ$  around the systems center

### 3.4 All (magnet, optics, detector)

In this part, as shown in Figure 26, the full possible effect due to gravity is simulated. This means that the magnet is turned in one direction around the point where the drive system is mounted to the support structure, and the XMM optics, together with the detector, are turned in the other direction around the same angle  $\alpha$ .

The efficiency loss due to this deformation can be seen in Figure 27.

In Figure 28, the distribution at the focal plane is shown for the same rotation angle of  $\alpha = -0.06^\circ$  as in Figure 25. In comparison, it can be seen that if the detector is

moved from its optimal position with the support structure, it also moves downwards from the focal spot.

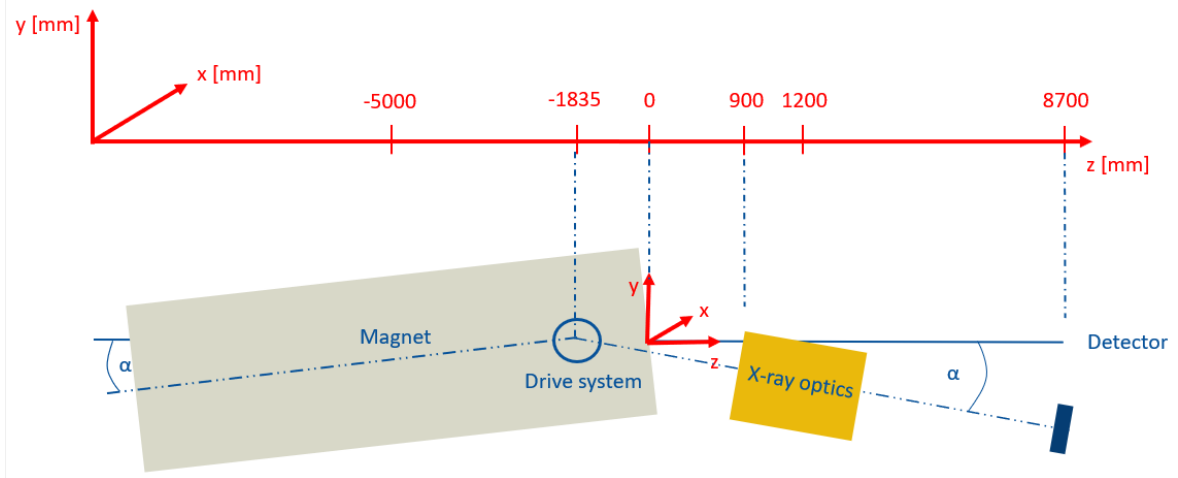


Figure 26: Coordinate system with the possible full effects due to gravity

### Relative Efficiency Comparison

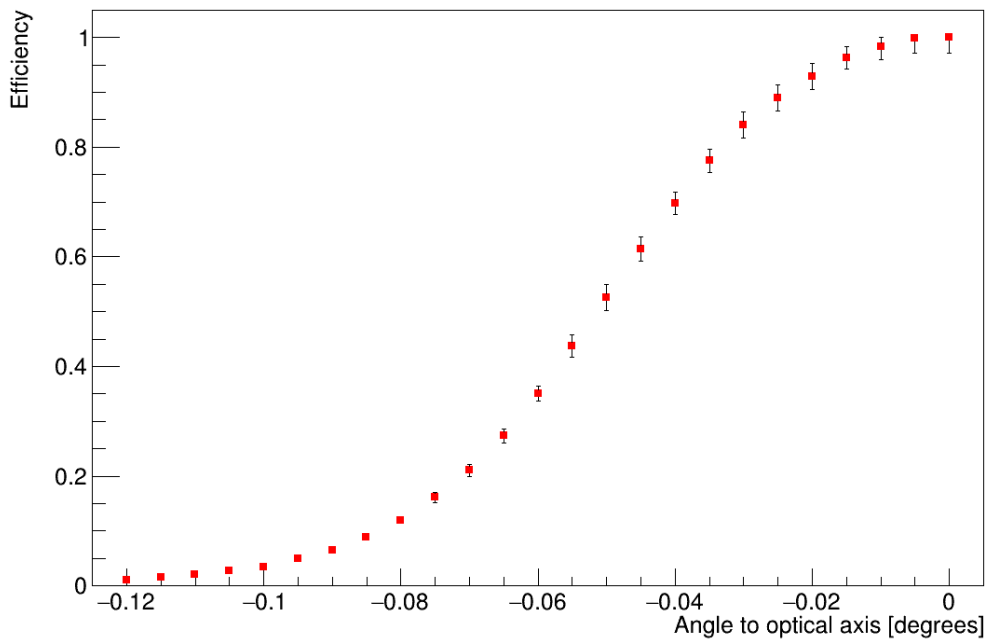


Figure 27: Efficiency of the whole setup depending on the angle it is turned around its own center in a downwards banana shape. 99% efficiency reached at  $\alpha = -0.01^\circ$  and 95% efficiency reached at  $\alpha = -0.018^\circ$  ( $\Delta y = -3.33$  mm at  $z = 8.7$  m and  $\Delta y = -2.58$  mm at  $z = -10$  m)

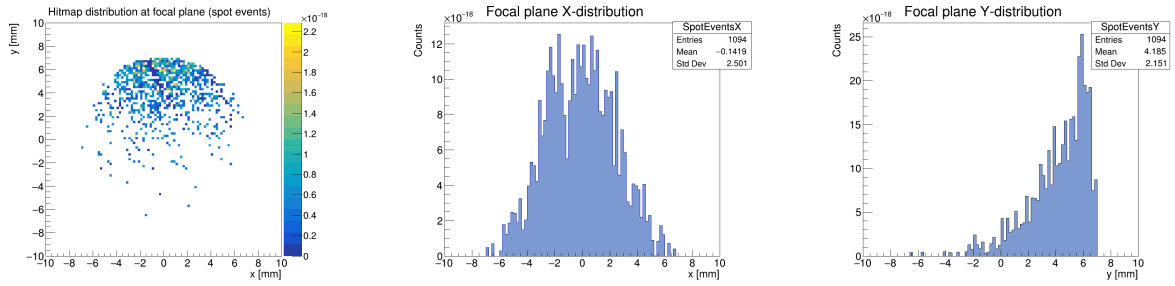


Figure 28: Distribution at the focal plane at a rotation of magnet, optics and detector of  $\alpha = -0.06^\circ$  around the systems center

The two previously described effects of the movement of the focal spot due to gravitational effects could be compensated by moving the detector. A small study of the possibly corrective distance  $\Delta y$  is shown in Figure 29. On the left, the downward movement of the focal spot from the original position is depicted (the detector in original position can be seen in Figure 23). In the right graph, the upward movement by which the detector would have to be corrected from the support structure (the support structure position can be seen in Figure 26) depending on the rotation angle is shown. This might be a more practical assessment as the distance from the bent support structure can be measured easier.

Figure 30 shows the efficiency due to gravitational effects of the whole system where the detector is corrected to be in the optimal position depicted in Figure 29.

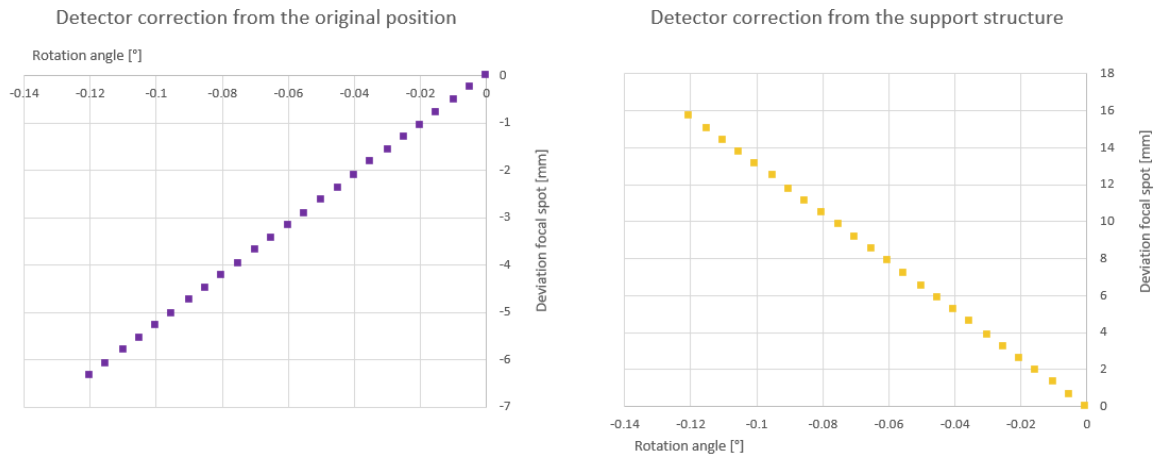


Figure 29: The distance in y-direction by which the detector would have to be corrected from the original (prev. also optimal position) and the support structure for the focal spot to be in the detector window center depending on the angle  $\alpha$  by which the magnet and the optics are rotated

### Relative Efficiency Comparison

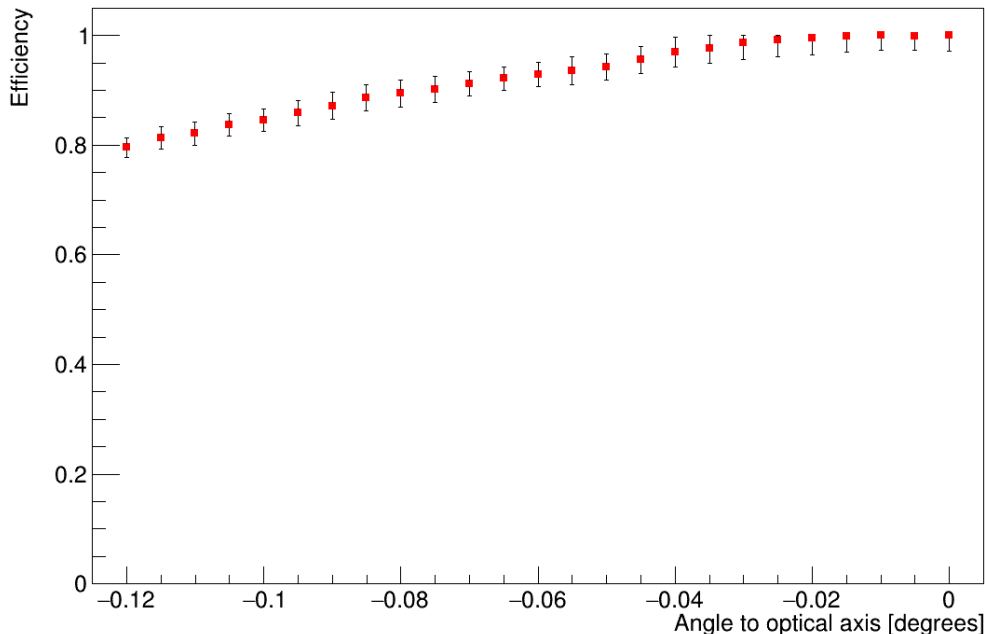


Figure 30: Efficiency of the whole setup depending on the angle it is turned around its own center in a downwards banana shape while the detector is corrected to be where the focal spot is. 99% efficiency reached at  $\alpha = -0.025^\circ$  and 95% efficiency reached at  $\alpha = -0.049^\circ$  ( $\Delta y = -9.03$  mm at  $z = 8.7$  m and  $\Delta y = -7.00$  mm at  $z = -10$  m)

### 3.5 Results gravitational effects

In the following Table 2 and 3, the angles  $\alpha$  are displayed as the rotation angles around the point where the drive system is mounted to the support structure where the efficiency of the system is 99% or 95%. Below each  $\alpha$  is the value  $\Delta y$  as the distance in y-direction from the optimal position at the respecting far side of the system for comparison with the values in Figure 18.

It is recognizable that the acceptance parameters are bigger when the detector is not moved with the system, as can be seen in the central column. To archive this, the detector position would have to be corrected in relation to the system structure while the system is operating. This is a consideration that has to be taken into account while reviewing this data.

Another consideration is that the misalignment, i.e. the internal rotation or movement of the components as depicted in Section 2, would, of course, change these acceptance values.

Magnet side				
	Magnet	Magnet and optics	All	Detector corrected
$\alpha(99\%)$ [°]	-0.19	-0.016	-0.01	-0.025
$\Delta y(99\%)$ [mm]	-27.25	-2.23	-1.39	-3.58
$\alpha(95\%)$ [°]	x	-0.035	-0.018	-0.049
$\Delta y(95\%)$ [mm]	x	-4.94	-2.58	-7.00

Table 2: The values of  $\alpha$  and derived from that the  $\Delta y$  at the furthest point from the center of the setup on the magnet side where the flux in the detector is 99% and 95% from the flux at the optimal position

Detector side				
	XMM optics	Magnet and optics	All	Detector corrected
$\alpha(99\%)$ [°]	-0.0175	-0.016	-0.01	-0.025
$\Delta y(99\%)$ [mm]	-3.22	-2.87	-1.8	-4.61
$\alpha(95\%)$ [°]	x	-0.035	-0.018	-0.049
$\Delta y(95\%)$ [mm]	x	-6.38	-3.33	-9.03

Table 3: The values of  $\alpha$  and derived from that the  $\Delta y$  at the furthest point from the center of the setup on the detector side where the flux in the detector is 99% and 95% from the flux at the optimal position

### 3.6 Overall rotation of the setup

Here the whole system is rotated with regard to the optimal position. This way, the sun is not anymore on a line with the setup. In Figure 31, the concept of the overall over rotation is shown where the sun is on the solid blue line. Figure 32 shows the overall rotation downwards (pitch), and Figure 33 is the same for the overall rotation sideways (yaw).

This is very similar to the previous approach because the optics and detector move the same, but the magnet rotates together with them instead of in the other direction.

There is a very small difference between the two rotation directions due to the inhomogeneous magnetic field but not in a significant way.

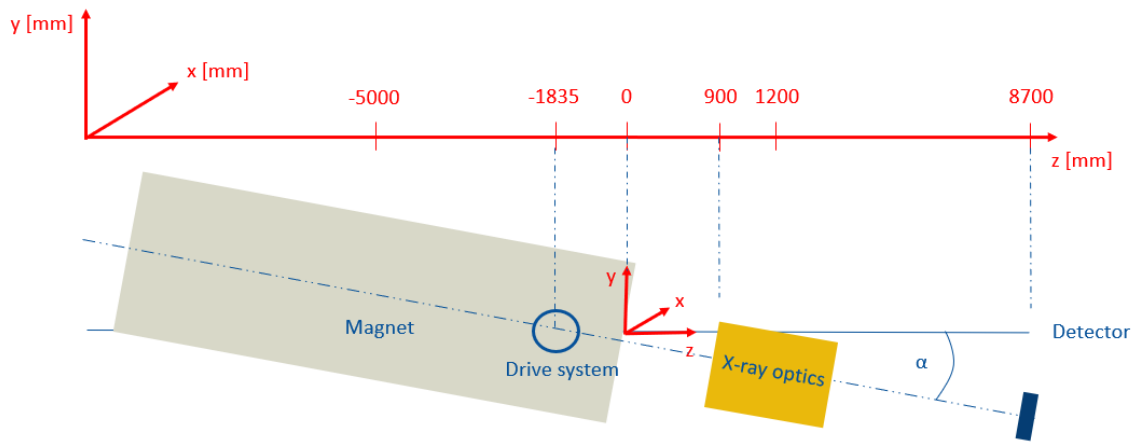


Figure 31: Coordinate system with the over rotation of the system

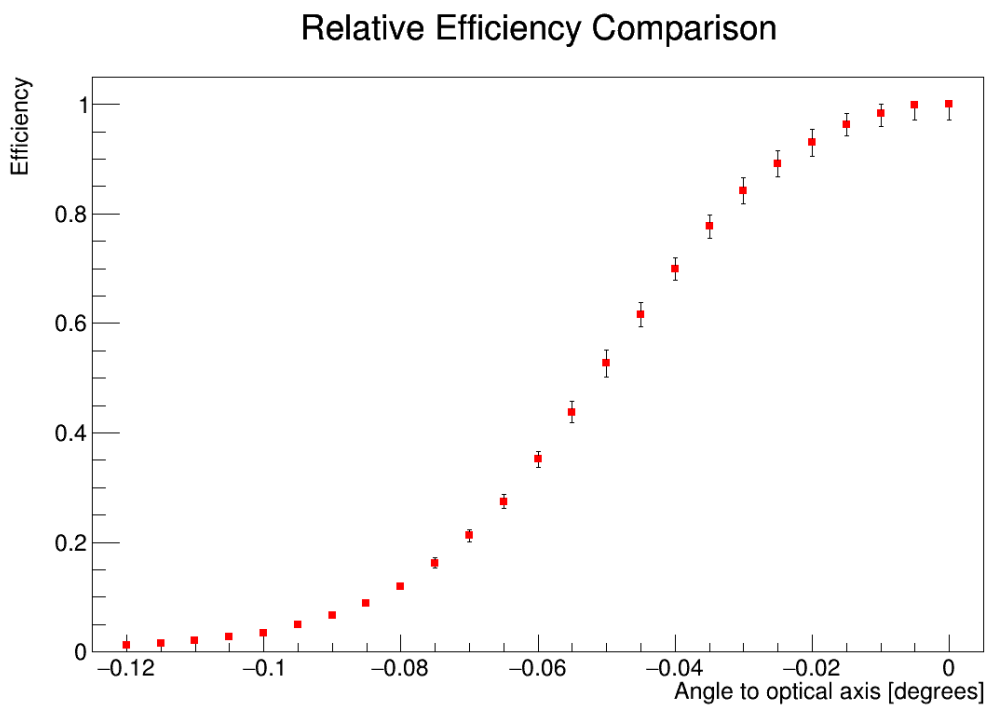


Figure 32: Efficiency of the whole system depending on its angle from the optimal position downwards (pitch). 99% efficiency reached at  $\alpha_{\text{pitch}} = -0.0098^\circ$  and 95% efficiency reached at  $\alpha_{\text{pitch}} = -0.0182^\circ$

### Relative Efficiency Comparison

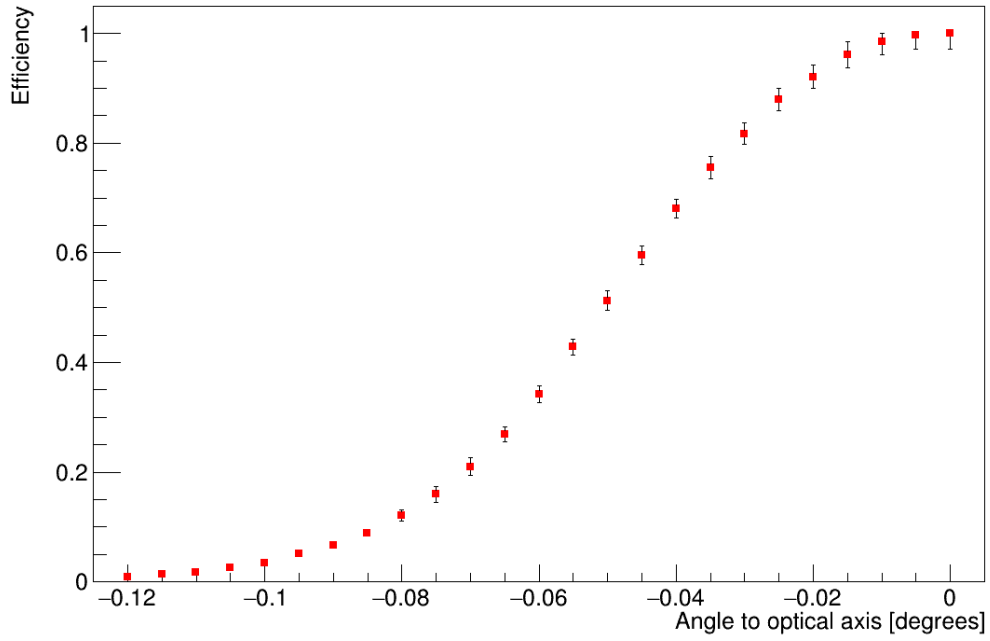


Figure 33: Efficiency of the whole system depending on its angle from the optimal position sideways (yaw). 99% efficiency reached at  $\alpha_{yaw} = -0.0095^\circ$  and 95% efficiency reached at  $\alpha_{yaw} = -0.0171^\circ$

## Appendix

Following the s-function in equation 1 the error of x at 99% and 95% efficiency are calculated with the derivatives of the function. Rearranging the equation for x gives:

$$x(y) = \sqrt{2}\sigma \cdot \operatorname{erf}^{-1} \left( \frac{y - 0.5A - B}{0.5A} \right) + \mu \quad (2)$$

The derivatives for all fit parameter are:

$$\frac{dx}{dA} = \frac{2.50663\sigma(B - y) \cdot \exp \left( \operatorname{erf}^{-1} \left( \frac{2(-0.5A - B + y)}{A} \right)^2 \right)}{A^2} \quad (3)$$

$$\frac{dx}{d\mu} = 1 \quad (4)$$

$$\frac{dx}{d\sigma} = \sqrt{2} \cdot \operatorname{erf}^{-1} \left( \frac{2(-0.5A - B + y)}{A} \right) \quad (5)$$

$$\frac{dx}{dB} = \frac{2.50663\sigma(B - y) \cdot \exp \left( \operatorname{erf}^{-1} \left( \frac{2(-0.5A - B + y)}{A} \right)^2 \right)}{A} \quad (6)$$

And then:

$$\Delta x = \sqrt{\left( \frac{dx}{dA} \Delta A \right)^2 + \left( \frac{dx}{d\mu} \Delta \mu \right)^2 + \left( \frac{dx}{d\sigma} \Delta \sigma \right)^2 + \left( \frac{dx}{dB} \Delta B \right)^2} \quad (7)$$